

Electrophoretic mobility does not always reflect the charge on an oil droplet

V. Knecht^{a,*}, H.J. Risselada^b, A.E. Mark^c, S.J. Marrink^b

^a Max Planck Institute of Colloids and Interfaces, Science Park Golm, 14424 Potsdam, Germany

^b Groningen Biomolecular Sciences and Biotechnology Institute, and Zernike Institute for Advanced Materials, University of Groningen, Nijenborgh 4, 9747 AG Groningen, The Netherlands

^c School of Molecular and Microbial Sciences, University of Queensland, St Lucia, Brisbane, QLD 4072, Australia

Received 7 September 2007; accepted 23 October 2007

Available online 3 December 2007

Abstract

Electrophoresis is widely used to determine the electrostatic potential of colloidal particles. Oil droplets in pure water show negative or positive electrophoretic mobilities depending on the pH. This is commonly attributed to the adsorption of hydroxyl or hydronium ions, resulting in a negative or positive surface charge, respectively. This explanation, however, is not in agreement with the difference in isoelectric point and point of zero charge observed in experiment. Here we present molecular dynamics simulations of oil droplets in water in the presence of an external electric field but in the absence of any ions. The simulations reproduce the negative sign and the order of magnitude of the oil droplet mobilities at the point of zero charge in experiment. The electrostatic potential in the oil with respect to the water phase, induced by anisotropic dipole orientation in the interface, is positive. Our results suggest that electrophoretic mobility does not always reflect the net charge or electrostatic potential of a suspended liquid droplet and, thus, the interpretation of electrophoresis in terms of purely continuum effects may need to be reevaluated.

© 2007 Elsevier Inc. All rights reserved.

Keywords: Electrophoresis; Electrokinetic phenomena; Zeta potential; Water structure; Molecular dynamics; Computer simulation

1. Introduction

Electrophoresis is the migration of an ion in a homogeneous electric field, the migration rate being proportional to the field applied [1]. The electrophoretic mobility of an ion (i.e., its migration rate divided by the intensity of the electric field in the surrounding medium) is proportional to the charge of the ion. Remarkably, neutral particles also show electrophoretic activity. Oil droplets [2–4] in the absence of surfactants at neutral or high pH show negative electrophoretic mobilities. Their electrophoretic mobilities correlate with pH and change sign at low pH [5,6]. This behavior is often explained in terms of the charging of oil droplets due to adsorption of hydroxyl (OH^-) or hydronium ions (H_3O^+) to the hydrophobic surface, leading to an excess of hydroxyl ions at neutral or high pH [7,8] or of hydronium ions at low pH. This view is supported by the obser-

vation that dispersion of oil droplets in water results in a change in the pH of the bulk water. A drop in pH is observed at high or neutral pH, and a rise in pH is observed at low pH [5,9]. Recent molecular dynamics simulations have also suggested that hydroxyl [10] or hydronium ion adsorption to a hydrophobic surface [11] can be induced by anisotropic water dipole orientation close to the surface. Remarkably, the isoelectric point (the pH value at which the electrophoretic mobility vanishes) and the point of zero charge (the pH value at which the dispersion of particles in water does not change the pH of the bulk water) do not coincide. For oil droplets, the isoelectric point is at about pH 3, whereas the point of zero charge is at about pH 6 [5]. At pH 6 where the surface charge suggested from the dispersion-induced pH shift is zero, oil droplets exhibit negative electrophoretic mobilities [5]. Alternative explanations for negative electrophoretic mobilities of oil droplets are that ionic impurities at the interface, or water ordering itself, could give rise to a negative electrostatic potential in the oil phase, driving the electrophoresis of oil droplets [5,8].

* Corresponding author.

E-mail address: vknecht@mpikg.mpg.de (V. Knecht).

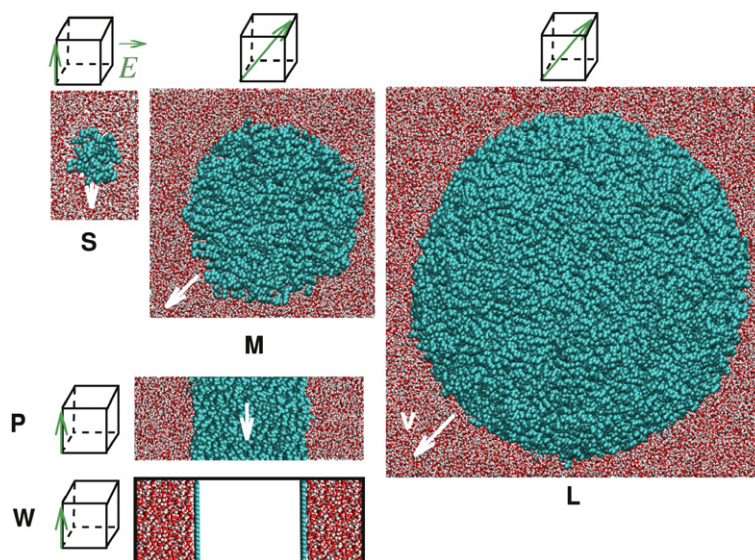


Fig. 1. The systems simulated were comprised of heptane (S, M, L, P, cyan or dark gray) or a hydrophobic wall (W, cyan or dark gray) and water (red or white). The heptane phase was either in the form of a droplet with radius 1.5 nm (S), 4.7 nm (M), or 8.2 nm (L), or a slab (P). S, M, and L show a section through the middle of the droplets. The direction of the external electric field (green or gray arrows) and the direction of the migration of the oil phase (white arrows) are indicated. (For interpretation of the references to color in this figure legend, the reader is referred to the web version of this article.)

Here we present results of molecular dynamics simulations of oil (heptane) droplets that show negative electrophoretic mobilities in the absence of hydroxyl or other ions. The results suggest that electrophoretic mobility does not solely reflect the net charge or electrostatic potential on a suspended particle. As such, the work challenges the current theory of electrophoresis, which is based primarily on simple continuum models, and suggests that dipolar ordering at hydrophobic interfaces might also play a role.

2. Methods

2.1. Simulation setup

The systems considered in this work are shown in Fig. 1 and specified in Table 1. Each system was composed of heptane or two hydrophobic walls and water. The heptane phase was in the form either of a droplet or of a slab in the xy plane. Heptane droplets of radius 1.5 nm (system S), 4.7 nm (system M), or 8.2 nm (system L), a slab (system P), or two hydrophobic walls (system W) were simulated under periodic boundary conditions. The droplet radius in system S was chosen to be somewhat larger than the width of a water/oil interface suggested from previous simulations [12]. The droplet size in system L was chosen to maximize size while keeping the computations feasible. The droplet radius in system M was chosen roughly equal to the arithmetic mean of the droplet radii chosen in systems S and L. In addition, a single heptane molecule in bulk water was simulated at equilibrium to study the structure of water in contact with heptane (system H). Here an octahedral box was used. For systems S, M, and L, rectangular (system S) or cubic (systems M and L) stacks of heptane molecules were placed in a rectangular or cubic box, respectively, with a distance of ~ 2.0 nm between the stack and the boundary of the box. The

Table 1

Systems simulated, oil droplets in water with radii 1.5 nm (S), 4.7 nm (M), and 8.2 nm (L), respectively, a heptane slab of thickness 6 nm (P), and two hydrophobic walls (W) in contact with water, or a single heptane molecule immersed in water (H)

System	N_H	N_W	R (nm)	$a \times b \times c$ (nm ³)
S	64	3859	1.5	$6.5 \times 4.5 \times 4.5$
M	1792	34,327	4.7	$11.6 \times 11.6 \times 11.6$
L	10,547	143,948	8.2	$19.6 \times 19.6 \times 19.6$
P	420	3418	–	$4.2 \times 4.2 \times 12.0$
W	–	3418	–	$4.3 \times 4.0 \times 12.3$
H	1	4147	–	56.3

Note. The systems were simulated at equilibrium and, except for system H, exposed to external electric fields. Given are the number of heptane molecules, N_H , the number of water molecules, N_W , the curvature radius, R , and the initial size of the simulation box, $a \times b \times c$. The number of wall atoms in system W was 720.

remaining space was filled with water molecules and the system was energy-minimized and simulated for 1 ns. In each case the heptane cluster adopted a spherical shape within ~ 300 ps. To generate system P, a periodic box of heptane molecules was energy-minimized and equilibrated to give the appropriate heptane density. The periodic box was extended in the z direction and the space created was filled with water molecules to create a two-dimensional slab of hexane in water. This system was energy-minimized and equilibrated. Systems S, M, L, and P were simulated at equilibrium and exposed to an external electric field. The electric fields were in the range 0.1–0.5 V/nm and applied in the positive x direction (systems S or P) or in the (1, 1, 1) direction (systems M and L) as depicted in Fig. 1 (green or gray arrows, color online).

To check for possible effects of the field direction, an additional simulation of system P was performed in which an electric field of 0.1 V/nm was applied in the positive y direction.

Note that the electric field in the system is dependent not only on the external field but also on the boundary conditions used to calculate electrostatic interactions [13]. The electric field in the water bulk (corresponding to the applied electric field in experiments, the *effective field*) was determined as described below. The box geometry and the direction of the electric fields were chosen to maximize the distance between the oil droplets and their periodic images in the direction of the field, allowing for the fact that an application of an electric field can induce the elongation of a oil droplet in the direction of the field. Such electrodeformation has been observed for lipid vesicles [14] and arises from Maxwell stress in the (high/low dielectric) water/alkane interface [15]. The systems were simulated for 40 ns (systems S, P, and W), 6.5 ns (systems M), or 1 ns (system L), at each field intensity. System H was simulated for 4 ns at equilibrium. To obtain sufficient statistics for a spatially resolved flow profile, the simulation of system P at an electric field of 0.3 V/nm was extended to 150 ns.

To determine the electrophoretic force between the heptane and the water phase, system P was also simulated at equilibrium and various field intensities subjecting the distance between the centers of mass of the heptane and the water phase in field direction, x , to a harmonic potential $V(x) = (k/2)x^2$ (umbrella potential) with a force constant $k = 10 \text{ J/mol nm}^2$. Similar simulations were performed for a system in which the heptane slab was replaced by two hydrophobic walls consisting of 360 atoms fixed on a triangular lattice with a lattice constant of 0.23 nm (Fig. 1 (W), system W). The distance between the walls was chosen such that the dimension of the hydrophobic phase normal to the field direction was similar to the thickness of the heptane slab in system P. The electrophoretic force F was determined from the time average of x , denoted as $\langle x \rangle$, according to

$$F = -k\langle x \rangle. \quad (1)$$

The systems described above were studied using molecular dynamics simulation techniques, which are based on iteratively solving Newton's equations of motion to propagate the system in time and semiempirical force fields to describe interatomic interactions, treating atoms as classical point masses [16]. The water was described using rigid water molecules with fixed charge distribution, employing the three-site simple point charge (SPC) model [17]. To test the effect of the water model, system P was also simulated at equilibrium and in an external field of 0.1 V/nm using the three-site SPC/E [18] and the four-site TIP4P [19] models. Heptane was described using the GROMOS-87 force field [20], in which the (nonpolar) hydrogen atoms of the heptane molecules are described using united atoms, whereas bond angles and torsions are described using standard potentials. For the wall atoms, Lennard-Jones parameters of the methylene groups of the GROMOS-87 force field were used. Each wall atom and united atom of a heptane molecule carried a partial charge of zero. Polarizability was not taken into account. In this model, an external electric field only interacts with the water molecules.

Full electrostatic interactions were considered using the particle mesh Ewald (PME) technique [21] using tinfoil boundary

conditions. To test the effect of the boundary conditions, system M was also simulated for 4 ns using PME using vacuum boundary conditions. All simulations were performed using GROMACS [22]. The lengths of covalent bonds in heptane molecules were constrained to ideal values using the LINCS method [23]. The bond lengths and bond angle in water were constrained using SETTLE [24]. In addition, the total mass of the molecule was redistributed in order to increase the mass of the hydrogen atoms, allowing the use of a 4-fs time step [25]. Heptane and water were separately coupled to an external temperature bath of 300 K using a Berendsen thermostat [26] with a coupling constant of 0.1 ps. The pressure was kept constant at 1 bar by coupling all directions simultaneously (systems S, M, and L), only the xy direction (interface plane, system P), or only the z direction (normal to interface plane, in the simulations using the umbrella potential for systems W and P), respectively, to a pressure bath using a Berendsen barostat [26] with a coupling constant of $\tau = 1.0$ ps. The coupling constants used for the thermo- or barostat were chosen to be weak enough to minimize the disturbance of the system and strong enough to keep the average temperature or pressure close to the desired value, based on empirical data [26]. In simulations at constant pressure, the box volume is not constant, but fluctuates over time. The relative fluctuations of the box volume were 0.2% and 0.1% for system S and M, respectively. Fluctuations in box size are realistic due to the finite (microscopic) size of the system. Relative fluctuations in volume vanish in the thermodynamic limit of an infinitely large (macroscopic) system. Atom coordinates and velocities of the systems were saved every 20 ps for analysis.

2.2. Analysis details

Analysis was performed omitting the initial 100 ps (system S), 300 ps (system M), 100 ps (system L), or 1500 ps (systems P and W), respectively, for equilibration. The electrophoretic mobilities were determined from the migration rate of the center of mass of the oil phase in the direction of the field. For the heptane droplets the absolute rate, and for the heptane slab the rate of migration relative to the center of mass of the water phase, were determined. For system P at an electric field of 0.3 V/nm, a spatially resolved flow pattern was determined from the final 110 ns of a 150-ns simulation. Here, the average velocity of atoms in field direction as a function of the distance s normal to the interface, was determined using a 0.6-nm bin width. Error bars for migration rates, flow profile, or electrophoretic forces (Eq. (1)) give the standard error from block averages obtained by dividing the trajectory into four segments. Electrophoretic mobilities were obtained from linear fits to the observed migration rates of the droplets as a function of the effective electric field. The effective electric field was taken as equal to the electric field in the water bulk. This assumption was made because in electrophoresis experiments, the oil fraction is very low (e.g., below 0.05 vol% in studies by Marinova et al. [8]). Hence, in experiment, the average electric field in the water/oil emulsion is approximately equal to the electric field in the water phase. According to continuum electrostatics, the

local electric field E in the water bulk is related to the polarization P_E in the water bulk via $P_E = \epsilon_0(\epsilon - 1)E$, where ϵ is the dielectric permittivity of water. For the molecular model used here, the polarization is given by $P_E = n\mu$, where μ is the average dipole moment of a water molecule in field direction, and n is the number density of water molecules. Using these equations, the effective electric field was determined from [13]

$$E = \frac{n\mu}{(\epsilon - 1)\epsilon_0}, \quad (2)$$

where n is the number density of the water molecules in the bulk, $n = 31 \text{ nm}^{-3}$. The value used for the dielectric permittivity ϵ of SPC bulk water was $\epsilon = 61$ [27].

For systems S and P at equilibrium, the density, ordering, and electrostatic properties of water were determined as functions of the coordinate s normal to the interface. Here the origin was set to the point at which the water density equaled half the bulk water density. Radial profiles for the oil droplets and profiles along the interface normal (z direction) for the planar interface or the wall were determined by dividing the distance scale into bins with a width of 0.01 nm. The profiles were smoothed using a Gaussian filter with a $\Delta s = 0.2$ nm bin width. To analyze the water ordering, the average dipole moment $\mu(s)$ of water molecules along the local interface normal was determined as a function of distance. The number densities n of atoms of water and heptane molecules (normalized to one) and the charge density $q(s)$ were evaluated in a similar manner. In particular, the charge density $q(s)$ was obtained from

$$q(s) = \left\langle \sum_{i: |s_i - s| < \Delta s/2} q_i / dV(s) \right\rangle. \quad (3)$$

Here, s_i denotes the position of atom i normal to the interface, q_i is the partial charge of atom i , $dV(s)$ denotes the volume element associated with the interval $[s - \Delta s/2, s + \Delta s/2]$, and $\langle \dots \rangle$ indicates time averaging. Note that the charge density was not determined from the divergence of the polarization, which would only be correct if water molecules were ideal dipoles. Rather, the full charge distribution was taken into account so that higher moments (quadrupole, etc.) were also considered. The electric field $E_0(s)$ along the local interface normal was determined from

$$E_0(s) = \frac{1}{\epsilon_0 s^2} \int_0^s q(s') ds' \quad (4)$$

for the oil droplets. This equation is the solution of the first Maxwell equation for radial symmetry, $(1/r^2)\partial(r^2 E_0(r))/\partial r = (1/\epsilon_0)\rho(r)$. This equation gives the electric field distribution in a sphere concentric with the oil droplet and enclosed by the simulation box, assuming approximate spherical symmetry in this spherical region. For the planar interface the field was determined from

$$E_0(s) = \frac{1}{\epsilon_0} \int_{s_0}^s q(s') ds'. \quad (5)$$

Here, s_0 denotes the position of the center of the oil slab. Note that the dielectric permittivity $\epsilon = 1$ was used in Eqs. (4)

and (5). This is correct for a molecular model of a dielectric where all charges are taken into account explicitly, in contrast to continuum electrostatics where a dielectric is modeled implicitly using a dielectric permittivity $\epsilon > 1$. The electrostatic potential $\phi(s)$ with respect to bulk water was determined from

$$\phi(s) = \int_s^{s_{\max}} E_0(s') ds'. \quad (6)$$

Here s_{\max} resides in the bulk water. Analysis of the average water dipole moment μ was restricted to regions with a water density larger than a fraction of 0.01 of the bulk density in order to ensure sufficient statistics.

Similar, for system H at equilibrium, the density, ordering, and electrostatic properties of water were determined as a function of the distance from the center of mass of a methyl(ene) group, s , averaged over all methyl(ene) groups. Here, the initial 100 ps were omitted for equilibration. The number density of water molecules was determined choosing a bin width of 0.03 nm. To analyze the water ordering, the average dipole moment $\mu(s)$ of water molecules along the distance vector was determined as a function of s denoting the distance between the centers of mass of the methyl(ene) group and the water oxygen. The charge density $q(s)$ was evaluated using Eq. (3). For the determination of $\mu(s)$ and $q(s)$, a bin width of 0.002 nm was chosen, and respective profiles were smoothed using a Gaussian filter with a $\Delta s = 0.12$ nm bin width. The electric field $E_0(s)$ along the distance vector was determined from Eq. (4).

3. Results

3.1. Oil droplets exhibit negative electrophoretic mobilities

The systems considered in this work were composed of heptane (Fig. 1, S, M, L, and P) or two hydrophobic walls (Fig. 1, W) and water. The heptane phase was in the form either of a droplet suspended in water (Fig. 1, S, M, L) or of a slab in contact with water (Fig. 1, P). In the simulations we observed that the oil droplets, when placed in a homogeneous electrostatic field (Fig. 1, S, M, L; green or gray arrows, color online) started to migrate in the negative field direction (Fig. 1, S, M, L; white arrows).

Fig. 2a shows the rate of migration of the oil phase for the different systems simulated as a function of the intensity of the electric field in the bulk water. The migration rates of oil droplets with radii 1.5 and 4.7 nm show a linear dependence on the field strength in accord with experiment [28]. Note that due to diffusion the migration rates at $E = 0$ appear nonzero. However, estimating the uncertainty in the migration rates due to diffusion as described in Section 2, we find that, within the statistical uncertainty, the migration rates do tend to zero at $E = 0$.

Oil droplets that were studied in experiment [4,8] are about two orders of magnitude larger than the oil droplets simulated in this study. Locally, the surface of the oil droplets studied experimentally is almost flat (compared with the molecular dimensions of the interface). To model this case, a heptane slab

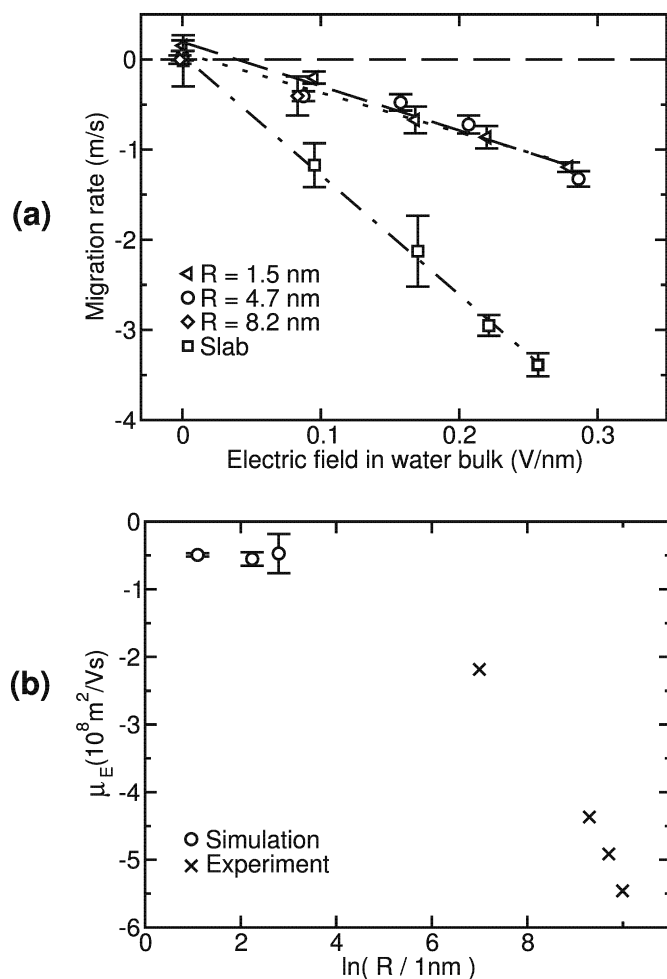


Fig. 2. (a) Migration rates v of heptane in water as a function of the effective electric field (see Fig. 1). For each system the data set and a linear fit are shown. (b) Electrophoretic mobilities μ_E of heptane droplets in water determined from the simulations, and of Nujol droplets in distilled water [29], as a function of the droplet radius R .

in contact with water was simulated (Fig. 1, P). The application of an electric field parallel to the heptane–water interfaces (Fig. 1, P; green or gray arrow, color online) induced a tangential movement of the two phases relative to each other (Fig. 1, P; white arrow, and Fig. 2a; squares). Again, the migration rates scaled linearly with the field intensity.

The simulations mimic conditions at the point of zero charge of oil droplets, pH 6 [5]. The electrophoretic mobilities of the heptane droplets in our simulations might be compared to the electrophoretic mobilities of oil droplets at pH 7, as electrophoretic mobilities of oil droplets at pH 6 and 7 are equal (within the experimental accuracy) [8]. Fig. 2b shows electrophoretic mobilities of heptane droplets determined from the simulations and electrophoretic mobilities of oil droplets in distilled water determined from experiment [29], as a function of radius. For droplets with radii in the order of micrometers a pronounced increase of electrophoretic mobilities with droplet size is observed in experiment. For droplets in the simulations with radii in the nanometer range, no clear size dependence is observed. Given the uncertainty in the simulations, it is not

possible to conclude if for droplets with radii in the nanometer range there is or is not a significant size dependence. Most importantly, the electrophoretic mobilities of the oil droplets in the simulations are of the same order of magnitude as those found in the experiment.

All simulation studies are model- and system-dependent. Control simulations have therefore been performed to check for possible effects due to the water model, the direction of the electric field, and the boundary conditions used to calculate electrostatic interactions (see Section 2). No significant effect on mobilities of the heptane phase was found.

In the interpretation of electrophoresis experiments, the solvent flow around a migrating particle is assumed to be laminar (i.e., not turbulent). Our systems are in the laminar regime, as suggested from an estimation of the order of magnitude of the Reynolds number, giving the ratio of inertial to viscous forces. The Reynolds number Re of a flow process is defined as

$$Re = \rho v L / \eta. \quad (7)$$

Here ρ is the density of the flowing liquid, v the characteristic velocity of the flow process, L the dimension of the object through or around which the fluid flows, and η the viscosity of the liquid. The flow process is laminar if Re is smaller than a critical value Re_{crit} depending on the flow process. The critical Reynolds number for the electrophoresis of the oil droplets in a periodic box in our simulations is expected to be in a range given by the Reynolds numbers for a sphere dragged through a liquid ($Re_{crit} \approx 350$ [30]) and a liquid flowing through a tube ($Re_{crit} = 2320$ [31]). An upper bound Re_{max} for the Reynolds numbers of our simulations can be obtained from the density of water, $\rho = 1000 \text{ kg/m}^3$, the maximal velocity observed in the simulations of the droplets, $v \approx 1.5 \text{ m/s}$, the dimension of the box normal to the flow direction for the largest system (system L), $L \approx 19.6 \times \sqrt{3} \text{ nm}$, and the viscosity of heptane at 25° , $\eta \approx 0.4 \text{ mPa s}$ [32] (the viscosity of heptane, being smaller than that of water [32], is used here to estimate an upper bound of Re). These values yield $Re_{max} \approx 0.1$. Our systems should thus be well into the laminar regime.

To induce significant electrophoretic motion on the time scale that could be simulated (tens of nanoseconds), high electric fields in the range 0.1–0.3 V/nm were applied (the values refer to the value of the electric field in the water bulk). These exceed those typically used in electrophoresis experiments [8] by several orders of magnitude. However, in recent microsecond electrophoresis studies of photoreaction intermediates, electric fields exceeding 0.01 V/nm have been used [33], and despite the relatively high field intensities used in these experiments, the migration rates were found to scale linearly with the field intensity. We note that the migration rates of the oil droplets observed in the simulations show a linear dependence on the field intensity, indicating that nonlinear effects are not significant. Recent molecular dynamics simulations of the electrophoresis of small single-stranded RNA oligomers [34] at field intensities similar to those used in the present study also show migration rates scaling linearly with the field intensity, with electrophoretic mobilities agreeing well with experiment. This suggests that the simulations performed at high electric

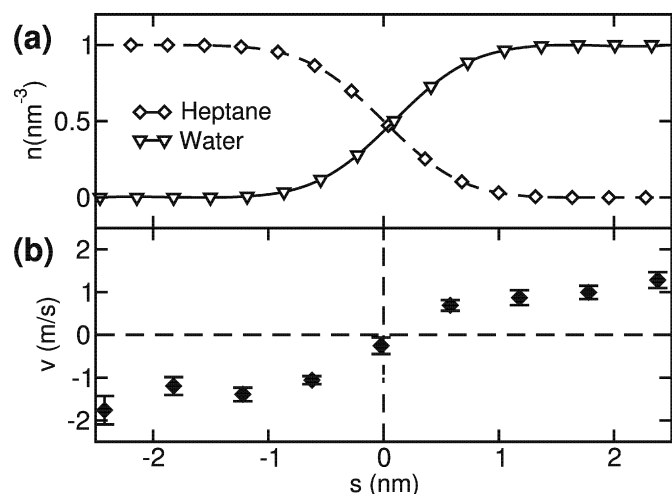


Fig. 3. Steady state properties for planar heptane/water interface parallel to an effective electric field of 0.26 V/nm. Shown are (a) the heptane and water density n and (b) the average velocity v in the field direction, as a function of the distance s normal to the interface.

field intensities can be directly related to the available experimental data. Furthermore, it gives confidence that the very good agreement in terms of both the sign and the order of magnitude of the electrophoretic mobilities of the oil droplets observed in the simulations is due to an appropriate representation of the underlying physical process and not artificial.

3.2. Shear in the water/oil interface

Fig. 3 shows steady state properties for the planar heptane/water interface parallel to an effective electric field of 0.26 V/nm. The heptane and water density (Fig. 3a) and the average velocity v in the field direction (Fig. 3b), are plotted as a function of the distance s normal to the interface. The data suggest that $v(s)$ exhibits (i) plateau regions in the bulk of heptane and water, and (ii) a smooth transition at the interface. These findings reveal that shear arises at the interface.

3.3. Electrostatic potential in oil phase is positive

To check if the negative electrophoretic mobilities of the heptane droplets arise from a negative electrostatic potential in the oil phase, the properties of water–heptane interfaces at equilibrium were analyzed. Fig. 4 shows the ordering of water and the electrostatic properties of a curved (radius 1.5 nm) and a planar heptane–water interface. In Fig. 4, the heptane and water densities (a), the average water dipole normal to the interface (b), the charge density (c), and the electrostatic potential (d) are shown as a function of the distance s normal to the interface. The same qualitative picture is obtained for the curved as for the planar interface. Fig. 4b shows the presence of a negative dipole moment for water molecules on the oil side of the interface (residing at negative s values). This indicates that water molecules close to the oil phase point with their hydrogen atoms toward the oil phase. Fig. 4c shows that a pseudo electric double layer of positive and negative charge emerges with the region of positive excess charge located close

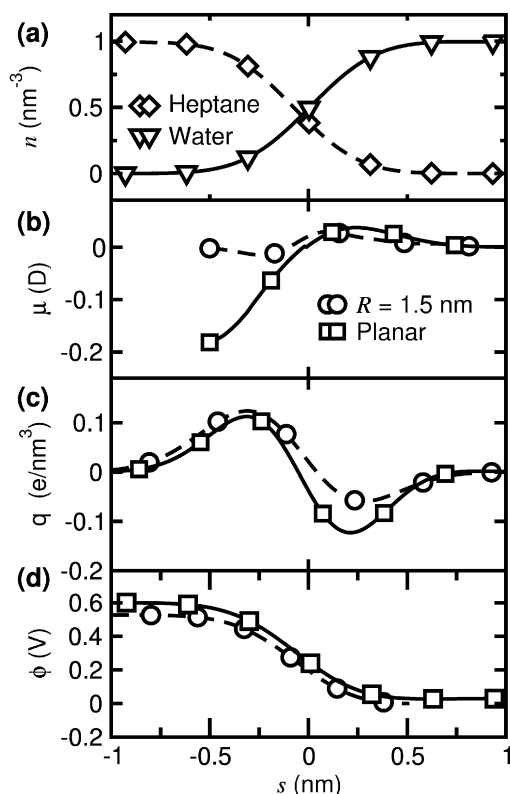


Fig. 4. Equilibrium properties of a curved (curvature radius 1.5 nm) and a planar water–heptane interface. Shown are (a) the heptane and water density n , (b) the average water dipole moment along the local interface normal (μ), (c) the charge density (q), and (d) the electrostatic potential (ϕ) as a function of the distance s normal to the interface.

to the oil phase. The term *pseudo electric double layer* is used to distinguish it from the term *electric double layer* commonly used to denote interfacial charge separation due to inhomogeneous distribution of free charges such as ions. In our system, charge separation arises from bound charges due to anisotropic dipole orientation. It is clear, however, that, independent of its origin, interfacial charge separation, as evident from Fig. 4c, will induce a difference in electrostatic potential between the two phases in contact. Fig. 4d shows that the electrostatic potential of the heptane with respect to the water phase is *positive*.

Previous studies of water/oil or water/vapor interfaces have yielded conflicting results for the sign of the electrostatic potential $\Delta\phi$ in the hydrophobic phase relative to the water phase. Theoretical estimates of $\Delta\phi$ induced by anisotropic dipole orientation were dependent on the water model as well as the method used to calculate $\Delta\phi$. A mean-field approach by Stillinger and Weber [35] in which a water molecule in a water/vapor interface was described as a point dipole and quadrupole within a region of slowly varying dielectric permittivity suggested $\Delta\phi > 0$. A similar model by Croxton in which a different quadrupole moment for water was used yielded $\Delta\phi < 0$ [36]. In molecular dynamics studies of a water/vapor interface by Matsumoto and Kataoka [37] and Barraclough et al. [38], $\Delta\phi$ was determined from the polarization density normal to the interface, yielding $\Delta\phi < 0$. Wilson et al. showed that it

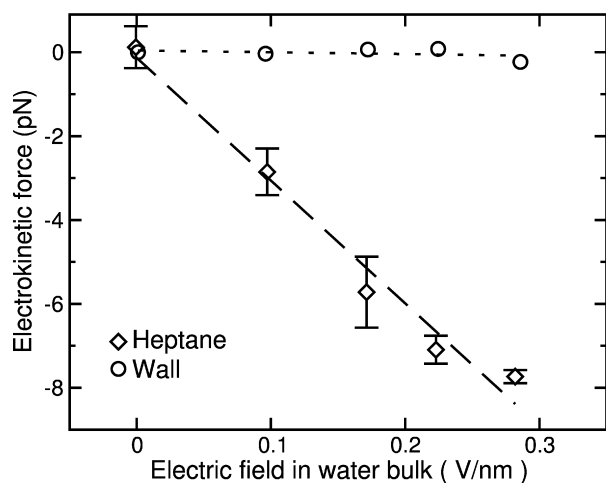


Fig. 5. Electrophoretic force between water and a heptane slab or a smooth hydrophobic wall (see Fig. 1) as a function of the effective electric field. For each system the data set and a linear fit are shown.

is essential to determine $\Delta\Phi$ by integrating the *charge density* normal to an interface, thus considering the quadrupole moment and the finite dimension of the water molecules, to obtain the correct sign of $\Delta\Phi$ from a simulation [39]. Molecular dynamics studies of a water/vapor interface yielded $\Delta\Phi < 0$ for the TIP3P water model [40] and $\Delta\Phi > 0$ for the TIP4P [39] or the SPC/E water model [41]. A molecular dynamics study of a water/decane interface yielded $\Delta\Phi \approx +0.4$ V for the SPC water model [12]. Recent molecular dynamics studies of a water/hexane interface using a polarizable water model yielded $\Delta\Phi \approx +0.1$ V for a fixed-charge hexane force field and $\Delta\Phi \approx +0.4$ V for a polarizable hexane force field [42].

Experimentally, $\Delta\Phi$ cannot be determined unambiguously. This is because the measured potential difference includes the difference in the chemical potential which is not easily estimated [1]. Experimental estimates of $\Delta\Phi$ for an air/water interface for example were mainly based on the changes in the potential with electrolyte concentration and range from -0.5 to $+1$ V (a survey is given in [43]).

3.4. Electrophoretic force requires interfacial roughness

Electrophoretic motion arises from a balance between a driving force we shall denote here as the *electrophoretic force* and a frictional force. The electrophoretic force between a heptane and a water slab in contact was determined by restraining the distance between the centers of mass of heptane and water in the field direction using a harmonic force. The force was determined from the deflection using Eq. (1). Fig. 5 shows the electrophoretic force as a function of the electric field which can be well fit using a linear function. The slope of the linear fit is $Q = -0.18(2)e$, where e denotes the elementary charge. Assuming Q to be proportional to the interfacial area, this corresponds to a pseudo-charge density of $\sigma = -0.011(1) e/\text{nm}^2$. In contrast, for water in contact with a hydrophobic wall, no significant electrophoretic force is detected.

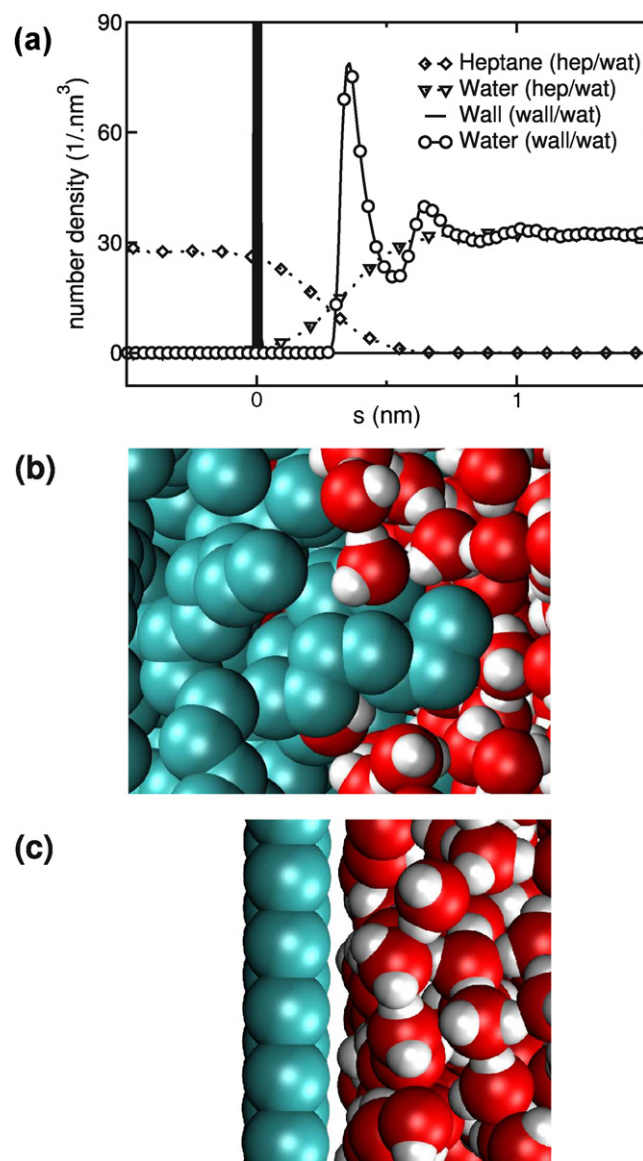


Fig. 6. Equilibrium properties of the interface between water and heptane or a smooth hydrophobic wall. (a) Water (and heptane) density as a function of the distance s normal to the interface. (b) Configuration of a water/heptane interface. (c) Configuration of a water in contact with a smooth hydrophobic wall. The representation is similar to that chosen in Fig. 1.

Fig. 6a shows a comparison between the equilibrium properties of the interface between water and heptane or the hydrophobic wall. Whereas the density of water in contact with heptane shows a smooth transition normal to the interface, a sharp transition and density oscillations are observed for water close to the wall. A similar density profile has been observed in a previous study of water in contact with a hydrophobic wall [10]. Fig. 1b shows a configuration of a water/heptane interface. It is evident that some interfacial heptane molecules protrude into the water phase such that the interface is rough on a molecular scale. In contrast, the wall/water interface is smooth on this scale. Comparison of Figs. 5 and 6 suggests that molecular roughness is required for electrophoretic forces between water and a hydrophobic phase.

4. Discussion

4.1. Simulations challenge current continuum picture

The simulation conditions for oil droplets in water chosen here are comparable to experimental conditions at the point of zero charge in the absence of electrolytes or ionic surfactants. At the point of zero charge, the surface concentrations of hydronium and hydroxyl ions in a water/oil interface are equal, and, in the absence of electrolyte ions or ionic surfactants, the surface charge of an oil droplet in water is zero.

The oil droplets in our simulations showed negative electrophoretic mobilities, in agreement with the experimental observation of negative electrophoretic mobilities for oil droplets at the point of zero charge. Our findings suggest that negative electrophoretic mobilities of oil droplets require neither the presence of ions nor a negative electrostatic potential in the oil phase. This in turn implies that the electrophoresis of a liquid droplet does not solely reflect the charge or electrostatic potential of the droplet, challenging the current theory of electrophoresis.

Electrophoresis of a colloidal particle is generally attributed to the presence of an electrical double layer in the interface creating a difference in the electrostatic potential between the two phases [28]. An electric field parallel to the interface induces shear stress and, hence, a flow of the suspending fluid relative to the particle. The electrophoretic mobility of a particle is expected to be proportional to the electrokinetic potential or zeta potential (the electrostatic potential on the shear plane, measured with respect to the bulk of the suspending medium). The zeta potential, conversely, is proportional to the net charge of the particle, denoting the sum of (i) the bare charge of the particle arising from ions or ionic groups attached to the surface and (ii) the charge of the part of the counterion cloud dragged along with the particle during electrophoresis, reducing the effective charge of the particle [44]. In our simulations of oil droplets in water in the absence of any ions or ionic molecules, the bare as well as the net charge of the oil droplets is zero. Furthermore, in a continuum description of the systems we have simulated, no charges would be present. In such a model, application of an external electric field would not result in any net nor even local forces. Hence, the electrophoretic mobility of the oil droplets would necessarily be zero.

In general, continuum theory predicts the electrophoretic mobility, net charge, and zeta potential of a particle to be equal in sign. The zeta potential inferred from electrophoresis experiments is generally considered to be a measure of the difference in the electrostatic potential in two phases in contact (*contact potential*). As noted above for a water/oil or a water/vapor interface, the contact potential itself cannot be determined unambiguously. This is because the measured potential difference includes the difference in the chemical potential, which is not easily estimated [1]. The above interpretation of electrophoretic mobility, however, is based on continuum theory. In particular, it ignores the fact that due to nanoscale dimensions of an interface, molecular details may play a significant role in determining electrophoretic mobility. Even though no molecules

in the system carry a net charge, the individual atoms in water molecules carry partial charges. The interaction of these partial charges with the external field will lead to local forces. Although the total charge of a water molecule is zero, a net translational force on interfacial water molecules could result from local gradients in water dipole energies. Our simulation results showing electrophoretic activity of oil droplets in water in the absence of any ions suggest this may be the case.

4.2. Dipolar ordering around a heptane molecule in water

The current continuum theory based interpretations of electrophoretic mobility implicitly assumes that mobility arises from the inhomogeneous distribution of free charges such as ions. Dipolar ordering in the interface that appears to be the primary origin of mobility in our system is not considered. Our results suggest that shear forces arise in the interface and not in the bulk, and molecular protrusions from the oil phase are crucial for electrophoretic forces between the oil and the water phase. To determine the structure of water in contact with a heptane molecule, a single heptane molecule in bulk water was simulated at equilibrium, and various properties of water were determined as a function of the distance from the center of mass of a methyl(ene) group. In Fig. 7, the water density (a), the average dipole moment of water molecules along the distance vector (b), the charge density (c), and the electric field along the distance vector (d), are shown as a function of distance. Four distance regions, I–IV, can be distinguished, where regions I–III contain the first hydration shell, and region IV shows bulk-like behavior. In region I, where the water density is low, a narrow subregion exists in which the water dipole is negative, i.e., pointing toward the methyl(ene) group. In contrast, the water dipole is positive everywhere in regions II and III containing the density maximum (region II) and a local density minimum (region III). The water ordering results in a strong positive charge in region I, a negative charge in region II, and a weak positive charge in region III. The dipolar ordering and charge distribution here are similar to the interfacial charge distribution shown in Fig. 4, except for the region of weak positive charge missing in the interfacial profiles. The inhomogeneous charge distribution results in local electric fields. A strong positive field between regions I and II, a negative electric field between regions II and III, and a weak positive field between regions III and IV are observed. In regions I and II, field intensities exceeding 4 V/nm, an order of magnitude larger than the intensities of the electric fields applied, are observed. Thus, interestingly, the field intensities applied were small compared to the intensities of the local electric fields from dipolar ordering at equilibrium.

4.3. Role of ions

The electrophoresis of oil droplets is pH-dependent. Clearly ions do also play a role in this system. Hydroxyl or hydronium ion adsorption onto a water–oil interface would be expected to change the contact potential between oil and water and hence the zeta potential of oil droplets in water. Hy-

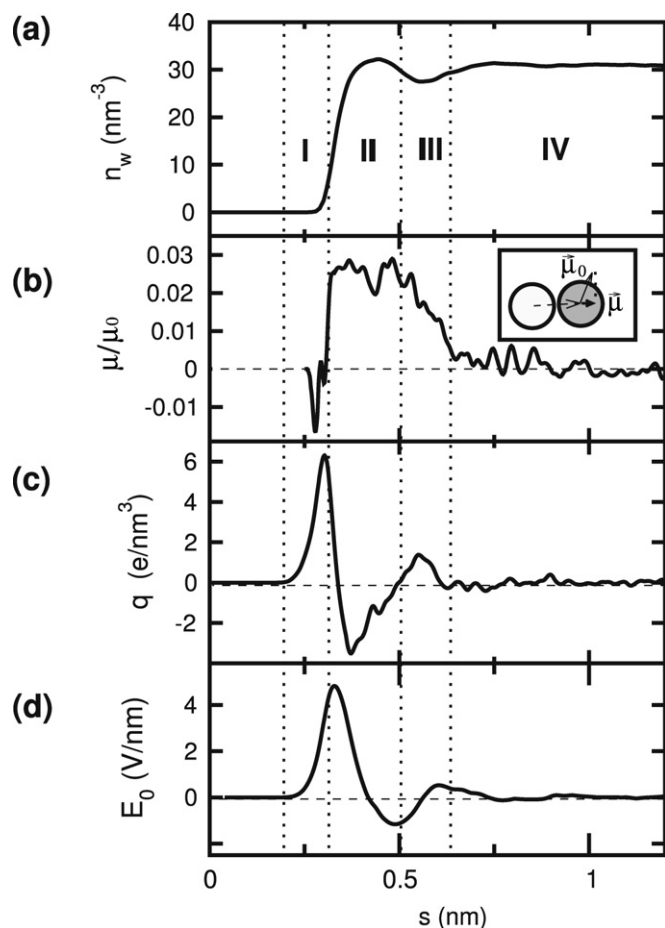


Fig. 7. Dipolar ordering and electrostatics around methyl(ene) groups of a single heptane molecule in water at equilibrium, as a function of distance s from the center of mass of the methyl(ene) group. The number density of water molecules (a), the average dipole moment μ of a water molecule along the distance vector, in fractions of the total dipole moment μ_0 of water molecule (b), the charge density q (c), and the electric field $E_0(s)$ along the distance vector are shown. The inset in (b) shows the definition of $\vec{\mu}$. Here, a methyl(ene) group and a water oxygen are depicted in light and dark gray, respectively.

droxyl or hydronium ion adsorption onto a water–oil interface would also change the spontaneous ordering of interfacial water dipoles. In the pH range between the isoelectric point, pH 3, and the point of zero charge, pH 6, oil droplets show negative electrophoretic mobilities despite an excess of hydronium ions adsorbed to the water/oil interface. We propose that for $3 < \text{pH} < 6$, the effect of the hydronium ions on the mobilities is overcompensated for by mobility associated with the water ordering and surface roughness. At the isoelectric point, the effects from hydronium ions and dipolar ordering/surface roughness-induced mobility compensate for each other. Here the positive surface charge from excess hydronium ions is expected to be equal in magnitude to the negative pseudo-charge from dipolar ordering/surface roughness-induced mobility, $\sigma = -0.011(1) \text{ e/nm}^2$, suggesting an excess of one hydronium ion per $91(1) \text{ nm}^2$ at the isoelectric point.

Electrophoretic mobilities of oil droplets in water suggest a change of -80 mV in the respective zeta potentials for a change in pH from 2 to 9 [8]. The respective change in the contact potential between oil and water is likely of the same order of

magnitude as the change in the zeta potential. This change in zeta potential is an order of magnitude smaller than the contact potential between oil and water arising purely from water ordering in the interface suggested by our simulations. Thus it appears that the structure of the interfacial water would determine the sign of the contact potential between oil and water in the whole pH range typically studied in electrophoresis measurements.

5. Conclusion

Electrophoresis experiments are extensively used to probe charge separation in interfacial regions of colloid systems [1]. Knowledge of such charge distributions is of major interest in colloid chemistry and electrochemistry. It is, for example, essential in understanding electrode kinetics, electrocatalysis, corrosion, adsorption, crystal growth, colloid stability, and flow behavior of colloidal suspensions [1]. We have shown that the electrophoretic mobility of a liquid droplet does not necessarily reflect the actual electrostatic potential or surface charge of the droplet. If true, the electrostatic potential of suspended droplets deduced from electrophoretic mobilities could thus be misleading, and the interpretation of electrophoresis experiments in terms of purely continuum effects and the neglect of the dipolar ordering may need to be reevaluated.

Acknowledgments

The authors thank M. Deserno, J.B.F.N. Engberts, R. Zangi, B.L. de Groot, H.J.C. Berendsen, M. Müller, and J. Menche for useful discussions. This project was funded by the From Molecule to Cell program of the Netherlands Organization for Scientific Research (NWO), Grant 80547091.

References

- [1] R.J. Hunter, *Zeta Potential in Colloid Science*, Academic Press, London, 1981.
- [2] J.C. Carruthers, *Trans. Faraday Soc.* 34 (1938) 300–307.
- [3] W. Dickinson, *Trans. Faraday Soc.* 37 (1941) 140–147.
- [4] A.J. Taylor, F.W. Wood, *Trans. Faraday Soc.* 53 (1957) 523–529.
- [5] J. Drzymala, Z. Sadowski, L. Holysz, E. Chibowski, *J. Colloid Interface Sci.* 220 (1999) 229–234.
- [6] C. Yang, T. Dabros, D.Q. Li, J. Czarnecki, J.H. Masliyah, *J. Colloid Interface Sci.* 243 (2001) 128–135.
- [7] K.A. Karraker, C.J. Radke, *Adv. Colloid Interface Sci.* 96 (2002) 231–264.
- [8] K.G. Marinova, R.G. Alargova, N.D. Denkov, O.D. Velev, D.N. Petsev, I.B. Ivanov, R.P. Borwankar, *Langmuir* 12 (1996) 2045–2051.
- [9] J.K. Beattie, A.M. Djerdjev, *Angew. Chem. Int. Ed.* 43 (2004) 3568–3571.
- [10] R. Zangi, J.B.F.N. Engberts, *J. Am. Chem. Soc.* 127 (2005) 2272–2276.
- [11] M.K. Petersen, S.S. Iyengar, T.J.F. Day, G.A. Voth, *J. Phys. Chem. B* 108 (2004) 14804–14806.
- [12] A.R. van Buuren, S.J. Marrink, H.J.C. Berendsen, *Colloids Surf. A Physicochem. Eng. Aspects* 102 (1995) 143–157.
- [13] M. Neumann, *Mol. Phys.* 50 (1983) 841–858.
- [14] E. Neumann, S. Kakorin, K. Toensing, *Faraday Discuss.* 111 (1998) 111–125.
- [15] M. Winterhalter, W. Helfrich, *J. Colloid Interface Sci.* 122 (1988) 583–586.
- [16] W.F. van Gunsteren, D. Bakowies, R. Baron, I. Chandrasekhar, M. Christen, X. Daura, P. Gee, D.P. Geerke, A. Glättli, P.H. Hünenberger, M.A.

- Kastenholz, C. Ostenbrink, M. Schenk, D. Trzesniak, N.F.A. van der Vegt, H.B. Yu, *Angew. Chem. Int. Ed.* 45 (2006) 4064–4092.
- [17] J. Hermans, H.J.C. Berendsen, W.F. van Gunsteren, J.P.M. Postma, *Biopolymers* 23 (1984) 1513–1518.
- [18] H.J.C. Berendsen, J.R. Grigera, T.P. Straatsma, *J. Phys. Chem.* 91 (1987) 6269–6271.
- [19] W.L. Jorgensen, J.D. Madura, *Mol. Phys.* 56 (1985) 1381–1392.
- [20] W.F. van Gunsteren, H.J.C. Berendsen, *GROMOS-87 Manual*, BIOMOS b.v., Groningen, The Netherlands, 1987.
- [21] T. Darden, D. York, L. Pedersen, *J. Chem. Phys.* 98 (1993) 10089–10092.
- [22] D. van der Spoel, E. Lindahl, B. Hess, G. Groenhof, A.E. Mark, H.J.C. Berendsen, *J. Comput. Chem.* 26 (2005) 1701–1718.
- [23] B. Hess, H. Bekker, H.J.C. Berendsen, J.G.E.M. Fraaije, *J. Comput. Chem.* 18 (1997) 1463–1472.
- [24] S. Miyamoto, P.A. Kollman, *J. Comput. Chem.* 13 (1992) 952–962.
- [25] K.A. Feenstra, B. Hess, H.J.C. Berendsen, *J. Comput. Chem.* 20 (1999) 786–798.
- [26] H.J.C. Berendsen, J.P.M. Postma, W.F. van Gunsteren, A. Di Nola, J.R. Haak, *J. Chem. Phys.* 81 (1984) 3684–3690.
- [27] T.N. Heinz, W.F. van Gunsteren, P.H. Hünenberger, *J. Chem. Phys.* 115 (2001) 1125–1136.
- [28] M. von Smoluchowski, in: L. Graetz (Ed.), *Handbuch der Elektrizität und des Magnetismus*, Verlag von Johann Ambrosius Barth, Leipzig, 1921, pp. 366–428.
- [29] M. Mooney, *Phys. Rev.* 23 (1924) 396.
- [30] C. Gerthsen, H.O. Kneser, H. Vogel, *Physik*, 16th ed., Springer-Verlag, Berlin/Heidelberg/New York, 1989.
- [31] R.Kh. Mullakhmetov, N.N. Rybnikov, *J. Eng. Phys. Thermophys.* 68 (1995) 456–459.
- [32] D.R. Lide (Ed.), *Handbook of Chemistry and Physics*, 75th ed., CRC Press, Boca Raton, 1999.
- [33] M.L. Plenert, J.B. Shear, *Proc. Natl. Acad. Sci. USA* 100 (2003) 3853–3857.
- [34] I.C. Yeh, G. Hummer, *Biophys. J.* 86 (2004) 681–689.
- [35] F.H. Stillinger, T.A. Weber, *Phys. Rev. A* 28 (1983) 2408–2416.
- [36] C.A. Croxton, *Physica A* 106 (1981) 239–259.
- [37] M. Matsumoto, Y. Kataoka, *J. Chem. Phys.* 88 (1988) 3233–3245.
- [38] C.G. Barraclough, P.T. McTigue, Y. Leung Ng, *J. Electroanal. Chem.* 329 (1992) 9–24.
- [39] M.A. Wilson, A. Pohorille, L.R. Pratt, *J. Chem. Phys.* 88 (1988) 3281–3285.
- [40] S.E. Feller, R.W. Pastor, A. Rojnuckarin, S. Bogusz, B.R. Brooks, *J. Phys. Chem.* 100 (1996) 17011–17020.
- [41] S.J. Marrink, S. Marcelja, *Langmuir* 17 (2001) 7929–7934.
- [42] S.A. Patel, C.L. Brooks, *J. Chem. Phys.* 124 (2006), Art. No. 204706.
- [43] M. Paluch, *Adv. Colloid Interface Sci.* 84 (2000) 27–45.
- [44] D.F. Evans, H. Wennerstroem, *The Colloidal Domain: Where Physics, Chemistry, Biology, and Technology Meet*, second ed., Wiley-VCH, New York, 1999.